Geosci. Instrum. Method. Data Syst. Discuss., 4, 43–84, 2014
www.geosci-instrum-method-data-syst-discuss.net/4/43/2014/
doi:10.5194/gid-4-43-2014

Geoscientific Instrumentation Methods and Data Systems Discussions
Open Access

An initial investigation of the long-term trends in the fluxgate magnetometer (FGM) calibration parameters on the four Cluster spacecraft

L. N. S. Alconcel, P. Fox, P. Brown, T. M. Oddy, E. L. Lucek, and C. M. Carr

Imperial College London, London, UK

Received: 25 October 2013 – Accepted: 13 December 2013 – Published: 27 January 2014

Correspondence to: L. N. S. Alconcel (l.alconcel@imperial.ac.uk)

Published by Copernicus Publications on behalf of the European Geosciences Union.

Abstract

Over the course of more than ten years in operation, the calibration parameters of the outboard fluxgate magnetometer (FGM) sensors on the four Cluster spacecraft are shown to be remarkably stable. The parameters are refined on the ground during the rigorous FGM calibration process performed for the Cluster Active Archive (CAA). Fluctuations in some parameters show some correlation with trends in the sensor temperature (orbit position). The parameters, particularly the offsets, of the Spacecraft1 (C1) sensor have undergone more long-term drift than those of the other spacecraft (C2, C3 and C4) sensors. Some potentially anomalous calibration parameters have been identified and will require further investigation in future. However, the observed long-term stability demonstrated in this initial study gives confidence in the relative accuracy of the Cluster magnetic field data. For the most sensitive ranges of the FGM instrument, the offset drift is typically 0.2 nT yr^{-1} in each sensor on C1 and negligible on C2, C3 and C4.

1 Introduction

The Cluster mission (Escoubet, 1997) consists of four Earth-orbiting spacecraft flying in formation at variable separations (100–10 000 km). The science phase of the mission began in February of 2001 and is presently scheduled to continue until December 2016 (pending final confirmation by the European Space Agency). Mission scientists study small-scale plasma structures in space and time in key regions of the magnetosphere, including the solar wind, the bow shock, the magnetopause, the polar cusps, the magnetotail and the auroral zones (Walsh, 2010). Each spacecraft carries the same set of eleven instruments which detect spatial and temporal changes in the magnetosphere by measuring ambient electromagnetic fields and particle populations. FGM is a DC magnetometer used to measure the magnetic field vector at the instrument position (Balogh, 1997).

GID
4, 43–84, 2014

Each FGM instrument consists of two triaxial fluxgate sensors. They are boom-mounted to minimize interference from the spacecraft background magnetic field, and the outboard sensor at the end of the 5 m boom is designated as the primary sensor for science data. The sensors can be operated in several ranges depending on the spacecraft's location in the magnetosphere, covering magnetic field magnitudes from less than 1 nT to over 65 000 nT (see Table 1). Data are normally obtained at a rate of ∼ 22 vectors per second (Hz), designated as "normal mode", although this can be increased to ∼ 67 Hz for short periods to investigate a region or event of particular interest ("burst mode").

After the raw data are downlinked, they are processed into a usable format and the time at which the data were measured is reconstructed. They are subsequently calibrated, validated and processed into the final FGM data products which appear on the Cluster Active Archive (CAA) (Laakso, 2010). Submission to the CAA occurs once all of these procedures have been performed on one month's worth of data, which is divided into orbits, defined as the periods between successive periapses. Orbit period varies from 51 to 57 h depending on the phase of the mission, with the orbits shortening as the mission progresses.

The four Cluster spacecraft are magnetically very clean, giving a high level of confidence in the DC magnetic field data obtained by the FGM instruments. The combination of measurement and modelling on the ground with a rigorous magnetic cleanliness programme and final compensation for magnetic contributions means that the spacecraft field at the outboard magnetometer sensors should be less than 0.25 nT (Balogh, 1997). It is not possible to verify this in-flight, however.

The accurate calibration of the FGM instrument is critical for scientific investigations requiring high-accuracy vector magnetic field data, for the production of some data sets by other instrument (PEACE) and for the calibration of other instruments aboard the Cluster spacecraft (EFW, STAFF, WHISPER).

GID
4, 43–84, 2014

2 FGM calibration

In order to place the parameter trends into context, it is useful to describe briefly the calibration, validation and archiving procedures. These are described in detail elsewhere (Gloag, 2010).

2.1 Theory

The FGM magnetic field data are subject to several significant sources of error that must be corrected to yield the best results for use in scientific studies and for use by other Cluster instruments. In the coordinate transformation of the magnetic field data from the sensor measurement frame to the spacecraft reference frame (and hence to a geophysical frame), errors may arise due to incomplete knowledge of: (i) the orientation of the sensors' axes; (ii) the sensor offsets; (iii) the sensor gains.

The relationship between the measurement frame and the spacecraft reference frame is specified by a set of 12 parameters for each spacecraft, as shown in Eq. (1) below. The set consists of the sensor angles, gains and offsets. The calibration parameters then define a transformation of the following form.

$$\begin{pmatrix} B_{S_1} \\ B_{S_2} \\ B_{S_3} \end{pmatrix} = \begin{pmatrix} G_1 \sin\vartheta_1 \cos\varphi_1 & G_1 \sin\vartheta_1 \sin\varphi_1 & G_1 \cos\vartheta_1 \\ G_2 \sin\vartheta_2 \cos\varphi_2 & G_2 \sin\vartheta_2 \sin\varphi_2 & G_2 \cos\vartheta_2 \\ G_3 \sin\vartheta_3 \cos\varphi_3 & G_3 \sin\vartheta_3 \sin\varphi_3 & G_3 \cos\vartheta_3 \end{pmatrix} \begin{pmatrix} B_x \\ B_y \\ B_z \end{pmatrix} + \begin{pmatrix} O_1 \\ O_2 \\ O_3 \end{pmatrix} \quad (1)$$

(B_x, B_y, B_z) is the magnetic field vector in the spinning spacecraft coordinate system, where x is aligned along the spin axis of the spacecraft and y, z are located in the spin plane, forming an orthogonal triad. In this equation, $(B_{S_1}, B_{S_2}, B_{S_3})$ represents the magnetic field vector as measured in the non-orthogonal sensor coordinate system, where S_1, S_2 and S_3 point approximately along the spacecraft x, y and z axes respectively. The parameters describing the transformation are the offsets (O_i), gains (G_i), elevation angles (θ_i) and azimuthal angles (ϕ_i). The elevation angle is measured with respect to the spacecraft spin axis x; the azimuthal angle is measured around from the y axis in

GID
4, 43–84, 2014

the spin plane y–z. Figure 1 illustrates the relationship between two reference frames. The gains and angles in the coupling matrix orthogonalise, scale and orient the field measured by the sensors, while the offsets handle zeroing the sensors.

These calibration parameters were accurately measured on the ground at the Technical University of Braunschweig as part of the pre-flight calibration of FGM. *However, these parameters cannot be expected to remain constant over the time scale of the mission; thus, in order to maintain the quality of the measured magnetic field data, an in-flight calibration process is required.* As a mission consisting of multiple spinning spacecraft which spend significant portions of their time in the solar wind, Cluster represents an opportunity to bring several magnetometer calibration methods to bear. The in-flight calibration technique is based upon two distinct methods: a Fourier analysis method (Kepko, 1996), which recovers 8 of the 12 calibration parameters, and a solar wind analysis method, which recovers the spin axis offsets O_1 (Hedgecock, 1975). A brief description of the theory underlying these methods, together with a discussion of their limitations and constraints on their application, is given below. Note that in addition to being orthogonalised and transformed into spacecraft coordinates, the magnetic field components must also be despun. For the sake of brevity, the despinning procedure will not be outlined here.

2.2 Fourier analysis

The Fourier analysis is based on the procedure detailed in Kepko, 1996. When the magnetic field data are despun, errors in particular calibration parameters will produce coherent monochromatic signals at the first and second harmonics of the spin frequency (approximately 0.25 Hz and 0.5 Hz for the Cluster spacecraft). More specifically: errors in the spin plane elevation angles (θ_2, θ_3) and spin plane offsets (O_2, O_3) produce signals at the first harmonic in the spin plane components of the field; errors in the relative spin plane azimuthal angles ($\Delta\phi_{32}$) and relative spin plane gains (ΔG_{32}) produce signals at the second harmonic in the spin plane components of the field; and

GID
4, 43–84, 2014

errors in the spin axis elevation angle θ_1 and spin axis azimuthal angle ϕ_1 produce signals at the first harmonic in the spin-axis component of the field.

Fourier-transforming the despun data produces a set of equations containing the errors in the above calibration parameters, which can then be inverted to recover the values of those parameters. The errors in the remaining four parameters (G_1, O_1, G_3, ϕ_3) do not produce coherent signals in the despun data and so they cannot be recovered by this method. After the Fourier analysis, the residual signal power at the first and second harmonics of the spin frequency provides one of the measures by which the accuracy of the calibration can be judged.

2.3 Solar wind analysis

In general, the four Cluster spacecraft sample the solar wind from mid-December to mid-April, a period which is known as the "dayside" season. During this period, the magnetic field in the solar wind is used to adjust the offset (O_1) associated with the axis of the sensor that is aligned with the spin axis of the spacecraft. FGM is nearly always in Range 2 during these periods, so this is the only range for which this method can be used to refine the spin-axis offset. This procedure is based on the observation that fluctuations in the solar wind magnetic field are primarily rotational, which means that there should be no correlation between the spin-axis component of the magnetic field and the total field magnitude (Hedgecock, 1975).

The procedure works by searching through the spin-averaged data for rotational discontinuities. At these discontinuities, O_1 is adjusted to minimize the correlation between B_1 and $|B|$. In general, one month's worth of data is divided in half and adjustments are applied separately to the first and second halves of the month. The implementation of this procedure was originally developed by FGM Co-Investigators at UCLA (H. K. Schwarzl, K. Khurana, M. Kivelson, personal communication, 2005) who have collaborated with the FGM team on its implementation at Imperial College. A complete description of the theory underlying this method can be found in Hedgecock, 1975.

GID
4, 43–84, 2014

From mid-April to mid-December the four Cluster spacecraft sample the Earth's magnetotail, a period which is known as the "nightside" or "tail" season. The technique described above cannot be applied to this data to adjust the spin axis offset. A simple linear interpolation of the offset between the last solar wind measurement in mid-April and the first solar wind measurement in mid-December is performed instead. This method likely masks the natural variation in the offset during these periods.

2.4 Range changes

When the FGM switches between ranges (Table 1), the magnetic field components are not precisely equal on either side of the change, due to differences in calibration between different ranges. In order to mitigate this, adjustments are performed to the remaining parameters not determined by either of the above procedures; namely O_1 (Ranges 3 and above), G_1, G_3 and ϕ_3. These parameters are adjusted from their measured values on the ground in order to minimize the discontinuities in the field components that occur at the range change. In common with the solar wind analysis, the implementation of this procedure was originally developed by FGM Co-Investigators at UCLA (personal communication, H. K. Schwarzl, K. Khurana, M. Kivelson, 2005) who have also collaborated with the FGM team on its implementation at Imperial College.

2.5 Validation and archiving

Once the calibration procedure has been completed, visual inspection of the calibrated data is carried out as a quality-control step. The accuracy of the calibration parameters recovered by the Fourier analysis method manifests itself in the signal power at the spin frequency in the processed data. The accuracy of the spin axis offset recovered by the solar wind method manifests itself in the spread exhibited between the four spacecrafts' spin axis data in the solar wind. The limitations of the calibration procedures mean that the quality of the final calibration can vary from month to month. Data intervals which do not meet the minimum standard for calibration quality are flagged in caveat

GID
4, 43–84, 2014

files which accompany the FGM data products on the CAA. Additionally, a calibration file for each orbit is produced. They are made available to investigators on the CAA, but since the FGM data products are already calibrated, they simply list the calibration parameters for each range in the orbit. The CAA web site (http://caa.estec.esa.int/caa/) gives researchers access to the data from all of the instruments on board Cluster from the start of the mission. Documentation and software tools are also downloadable.

2.6 Application and limitations of the calibration procedures

The parameters recovered by the Fourier analysis method are resolved most frequently; in practice, once per orbit. The remaining parameters are determined less often. Accurate determination of the spin axis offset by the solar wind method requires a minimum of 20 h of good quality solar wind data. Accordingly, during the dayside season, the spin axis offset is typically only determined twice per month. The range jump correction is usually performed once per month.

It is frequently the case that the spin axis parameters recovered by the Fourier analysis method have produced an inferior calibration to that obtainable by using calibration parameters from a previous orbit, as measured using the criterion of the signal power at the spin frequency. Accordingly, in such cases, multiple spin axis calibrations were substituted, and the set of parameters which produced the minimum spin power in the spin axis data was chosen as the final calibration.

The accuracy of the recovered parameters is strongly dependent upon the quality of the data available. Excessive signal noise, data gaps, etc. can all affect the efficacy of the calibration procedures. Periods of unavoidably poor calibration are flagged in FGM's CAA caveat files.

The original Cluster mission has been extended several times and utilised manoeuvres to configure a range of different spacecraft constellations. Trajectories bringing the spacecraft closer to the Earth than originally foreseen necessitated the use of the full instrument ranging capability. From November 2000 to October 2006, Ranges 2–4 (see Table 1) were in regular use. Starting in November 2006, Range 5 entered routine use.

GID
4, 43–84, 2014

Starting in May 2008, Range 6 entered routine use. Starting in December 2009, Range 7 entered routine use. Neither Range 6 nor Range 7 was originally intended for use during the nominal mission hence these ranges were not fully calibrated on-ground. The entry of the spacecraft into the inner magnetosphere and auroral acceleration zone in the extended mission phases meant that the total field magnitude exceeded the capacity of Range 5. The calibration parameters for Range 6 and Range 7 are tied to those of Range 5, as only partial ground calibration information was available for them.

3 Long term trends in FGM parameters

Having applied the above described calibration methods to the Cluster FGM data set over a period of 11 yr, we considered it valuable to begin an examination of the long-term behaviour of the FGM calibration parameters. Such a survey serves several purposes:

- It allows us to examine the long-term measurement stability of the FGM instrument. Such stability has been observed in other space-based fluxgate magnetometers such as those aboard the CHAMP and THEMIS satellites (Auster, 2008 and Yin, 2011).
- It allows us to quickly identify periods where the calibration parameters have anomalous values, flagging data that may need to be revisited to see if the calibration can be improved.
- It allows us to examine whether or not it is possible to correlate variations in calibration parameters with instrument and spacecraft events, particularly FGM instrument house-keeping telemetry.
- It gives some indication of the validity of interpolating the spin axis offsets across the tail season, by comparing the change in offset over the tail seasons with overall variation throughout the mission.

GID
4, 43–84, 2014

More generally, a time history of FGM calibration on board the four Cluster spacecraft represents a unique and valuable body of knowledge in the field of space magnetometry, which should serve to inform the planning of any similar future missions where accurate magnetometer data are important. The 11 yr of data discussed in this paper represents an opportunity to examine the results of a calibration campaign of unprecedented duration.

The remainder of this paper consists of several parts. The entire data set consists of the time series for each calibration parameter, covering the period from the start of the nominal mission at Orbit 93 (February 2001) to Orbit 1825 (February 2012) Presentation and discussion of the time series for each parameter is impractical, given that the complete data set encompasses 12 parameters for each of 6 ranges for each of the 4 Cluster spacecraft. Therefore, only a representative subset of the calibration parameters is discussed, highlighting what we consider the most significant features of the data set.

Additionally, a preliminary attempt has been made to correlate variation in the calibration parameters with instrument house-keeping telemetry. The instrument house-keeping consists of the following quantities: the FGM electronics box temperature located within the body of the spacecraft, the FGM outboard and inboard sensor temperatures on the boom, and the currents and the voltages of the electronics inside the electronics box Only the temperatures are discussed here.

3.1 Cross-spacecraft comparisons of instrument house-keeping telemetry values

The data displayed in Figs. 2 and 3 are for the outboard sensors on all of the spacecraft. They cover the period from February 2001 (Orbit 93) to August 2012 (Orbit 1889).

GID
4, 43–84, 2014

3.1.1 FGM outboard sensor temperature

The FGM sensors each contain a thermistor, which is independent of the FGM electronics and which is monitored by the spacecraft. Each sensor also contains a heater which can be operated independently from the remainder of the s/c electronics. Both heaters are powered through a single switch which is controlled by the spacecraft. The sensors have thermal insulation and their temperature can be expected to change at a maximum of $20\,^{\circ}\mathrm{C}\,\mathrm{h}^{-1}$. The sensors are monitored at intervals of the order of 30 min (FGM Instrument Users Manual). Although each of these values is monitored more frequently, a single averaged value has been shown for each orbit (51–57 h) in Fig. 2.

The outboard sensor temperatures for all four spacecraft show a cyclical fluctuation over the course of nightside-to-dayside transitions, becoming around 5 °C warmer during the peak of the dayside season.The spikes are due to long eclipse periods, during which the FGM is off. All sensors have undergone a warming trend over the course of the mission as shown in Fig. 2. Since the outboard FGM sensors are located on the ends of 5 metre booms, the warming and cooling cycle is most likely related to the spacecrafts' positions relative to the Sun during dayside and nightside seasons. The overall warming trend is likely related to the spacecrafts' positions relative to the Earth, as both periapsis and apoapsis have become lower over the course of the mission.

3.1.2 FGM electronics box temperature

The electronics box temperature is monitored from a thermistor located on the DC-DC converter card. This temperature can be expected to follow the temperature of the Main Equipment Platform. The upper and lower operational limits for the box temperature are [+60 °C, −25 °C]. If these limits are exceeded, the FGM instrument is powered off [9]. Although each of these values is monitored more frequently, a single averaged value has been shown for each orbit (51–57 h) in Fig. 3.

On all four spacecraft, the box temperature is about 21 °C, with a declining trend until around Orbit 600 (late May 2004), when it becomes cyclical as seen in the outboard

GID
4, 43–84, 2014

sensor temperature. The boxes undergo less dramatic warming than the outboard sensors of around 3 °C during the peak of the dayside season. This is likely due to their less exposed positions on the spacecraft body. The electronics boxes appear to be cooling over the course of the mission, with C1 and C3 cooling less dramatically than C2 and C4. The electronics boxes, due to their position on the spacecraft platform, are coupled to the spacecraft temperature much more strongly than the boom-mounted units. Changes in spacecraft heating strategy over the course of the mission, with more portions of the spacecraft being turned off during eclipses, are reflected in the electronics box temperature behaviour.

3.2 Inter-spacecraft calibration parameter comparisons by range

The data displayed are for the outboard sensors on all of the spacecraft and run from February 2001 (Orbit 93) to February 2012 (Orbit 1825).

3.2.1 Offsets

In Figs. 4 through 9, the individual offsets have been plotted for each range and spacecraft. The offsets in red have been applied to the spin-axis component of the magnetic field vector, while those in green and blue have been applied to the spin-plane components of the magnetic field vector. One offset value is applied across all data for a given range in an orbit. The spin-plane offsets are adjusted on a per-orbit basis no matter the phase of the mission. The spin-axis offsets, as mentioned in the Introduction, are adjusted on a biweekly or monthly basis during the dayside season when the spacecraft are in the solar wind and then interpolated between the end of one dayside season and the start of the next. The biweekly/monthly adjustment of the spin-axis offset gives a short, step-like appearance to the offset lines, while the interpolation method gives longer sloping steps for the seven or so months (around 100 orbits) that the spacecraft spend on the nightside portion of their tours.

GID
4, 43–84, 2014

Comparison of the smooth slopes of the interpolated offsets with the variability of the solar wind-adjusted offsets shows that the interpolation is probably masking the natural variability during the tail season. Orbits for which no FGM data were taken (and hence no calibration) have been omitted.

Over the course of the mission, offset drift is negligible in all components. The largest drifts in offsets take place on C1. C4 is the only other spacecraft with offsets that are comparable in magnitude to C1 in Ranges 2 through 5, but offset drift is still insignificant. Offset variation with temperature is about $0.2\,\mathrm{nT}^{\circ}\mathrm{C}^{-1}$ on C1 and $0.1\,\mathrm{nT}^{\circ}\mathrm{C}^{-1}$ on C2, C3 and C4.

For C1 in Range 2 (Fig. 4) there is a clear decreasing trend in the spin-axis offset O_1, which is visible even with the steps introduced by the interpolated values over the course of the mission. A decreasing trend is also seen in O_3. The total change is about 2 nT in O_1 and 1 nT in O_3. In O_2, the offset appears to increase by about 2 nT. On the other spacecraft, C2–C4, there is no overall drift, although some cyclical behaviour that may be related to instrument parameter cycles, particularly in the outboard sensor temperature, can be seen in C2 and C3.

Range 3 offset trends are very similar in magnitude and type to those observed in Range 2 (Fig. 5). This is not too surprising since the range change is achieved by switching a single feedback resistor. On C1, the decreases of 2 nT in the spin-axis offset O_1 and 1 nT in O_3 are observed, as is the 2 nT increase in O_2. On the other spacecraft, C2–C4, there is no overall drift, although some cyclical behaviour that may be related to instrument parameter cycles, particularly in the outboard sensor temperature, can be seen in C2 and C3. The offsets also appear to fluctuate more, particularly the spin-axis offset, early in the mission compared to Range 2. Some outlying values in the spin-axis offset for C2 will require further investigation.

Range 4 offset trends are similar in type to those observed in Range 2 (Fig. 6). The C1 drifts have increased by approximately an order of magnitude. The decrease of 2 nT has become 20 nT in the spin-axis offset O_1 and 1 nT in O_3 has become 8 nT. The 2 nT increase in O_2 has become 15 nT. On the other spacecraft, C2–C4, there

GID
4, 43–84, 2014

is no overall drift, although some cyclical behaviour that may be related to instrument parameter cycles, particularly in the outboard sensor temperature, can be seen on C2 and C3. The offsets fluctuate less, particularly the spin-axis offset, early in the mission compared to Range 3.

Since Range 5 did not enter routine use until late November 2006, Fig. 7 covers 800 orbits, or just over five years. C1 follows the trend seen in the lower ranges, where O_1 and O_3 are slowly decreasing and O_2 is slowly increasing. C2 shows slight signs of a cyclical trend like that observed in the outboard sensor and box temperatures. C3 shows strong signs of such a cyclical trend, while C4 shows the same stability and independence of instrument parameter trends exhibited previously. The potential correlation with instrument parameters in C2 and C3 merits further investigation in another section of the analysis.

Despite the limited data available in Range 6, the offset trends mirror those seen in the Range 5 data (Fig. 8). At present there are 500 orbits' worth, or just over three years, of data. As discussed in the Introduction, limited ground calibration information was available for this range since it was not originally intended for science investigation. Changes in the Range 6 parameters, including the offsets, are tied to changes in the Range 5 parameters, which were used during the initial calibration of Range 6 to help discover consistent values. It is therefore sensible that any potential correlation with other instrument parameters that were seen in Range 5 should also be observed in Range 6. As the mission continues and Range 6 is employed more regularly for lower periapsis passes, the consistency between Range 5 and Range 6 offsets should become clearer.

Insufficient data exists in Range 7 to distinguish many trends (Fig. 9). One exception is that large month-long deviations in a parameter, such as the one seen in the spin-axis offset around Orbit 1600 in C3, are paralleled by similar deviations in Range 6. Adjustments to the spin-axis offsets during range jump corrections are primarily responsible for such shifts, since a large change in the Range 6 spin-axis offset to eliminate R56

GID
4, 43–84, 2014

jumps is likely to result in the need for a large change in the Range 7 spin-axis offset to eliminate the R67 jumps.

At most (on C2 and C4) there are 60 orbits' worth, or five months, of data and at least (on C1) there are 36 orbit's worth, or three months, of data. Since the spacecraft are now off due to power-sharing issues during the lower periapsis passes that necessitated the use of Range 7, it is unlikely that this limited set will be expanded much. It will therefore not be possible to determine whether Range 7 follows the same trends as observed in the lower ranges for each spacecraft. Further discussion of this range has been omitted from the remainder of this article.

In Table 2, the mean value and standard deviations for the spin-axis and spin-plane offsets on each spacecraft over Orbits 93–1825 (February 2001 to February 2012) have been calculated. The standard deviations are fairly consistent between coordinates and across all ranges for C2, C3 and C4. With the exception of Range 7, the standard deviation for C1 is significantly larger, from two up to thirty times greater than the other spacecraft. This tallies with the observation of greater long-term drift in the offset parameters for C1 than in the other spacecraft.

3.2.2 Gains and angles

For most of the remaining calibration parameters, the fluctuations across the mission show no visible correlation with instrument parameters and no long-term trends. Mission averages for the parameters, which are the gains (G_i) and angles (θ_i and ϕ_i) will therefore be discussed in tabular form, with plots shown for exceptional cases.

In Table 3, the mean value and standard deviations for the spin-axis gain (G_1) and the difference of the spin-plane gains (ΔG_{32}) have been calculated. The change in the difference between the spin-plane gains is used as a calibration parameter. The final spin-plane gain values are therefore interdependent, which is why the difference is evaluated here. With two exceptions, notably the spin-axis gains for Ranges 3 and 4 on C1, there is little fluctuation in these parameters. The noted gains are shown in Fig. 10.

GID
4, 43–84, 2014

The two exceptional cases show similar behaviour. In Ranges 3 and 4 of C1, the fluctuations begin in orbits corresponding to late 2010, with no obvious correlation to other behaviour, through to February 2012.

One interesting behaviour not reflected in the gains table of averages and standard deviations occurs in Range 2 for all spacecraft. The spin-axis gain difference appears to undergo periodic increases in fluctuation, seemingly corresponding with the warming/cooling cycles observed in the instrument house-keeping temperature values, as shown in Fig. 11. The reason for this is unknown and merits future investigation.

In Table 4, the mean value and standard deviations for the elevation angles, theta, have been calculated. The levels of fluctuation in theta are consistent across ranges and spacecraft, with the exception of the spin-axis theta on C1 for all except Range 6 in which the levels are elevated. This might lead to the assumption that the C1 values are simply consistently elevated. The assumption is borne out when observing the theta values for Range 2 in all spacecraft as shown in Fig. 12. However, as shown in Fig. 13, an examination of all of the plots reveals that spikes of around 0.002 and 0.04° occur in Ranges 4 and 5 respectively for C1. This highlights the importance of examining the long-term trends in a number of ways. The variability of the spin-plane thetas has increased later in the mission.

In Table 5, mean value and standard deviations for the azimuthal angles, phi, have been calculated. The levels of fluctuation in phi are consistent across ranges and spacecraft, with the exception of the Range 5 in C1 and Range 2 on C3 in the spin-axis and Range 6 on C3 in the *y* coordinate of the spin-plane. As shown in Fig. 14, these are caused by spikes in the values for single orbits, indicating that the calibration for these orbits may need to be revisited.

3.2.3 Individual calibration and instrument house-keeping parameter comparisons

The calibrated offsets for C2 and C3 exhibited cyclical trends in some ranges that merit individual visual comparison with instrument parameters extracted from telemetry. The

GID
4, 43–84, 2014

cyclical trends become more obvious in the latter half of the mission, so Range 5 has been chosen as the primary example. On C2, O_1 and O_2 appear to track the electronics box and outboard sensor temperatures, rising and falling in the same cycle (Fig. 15). O_3 shows an inverted trend. On C3, all three offsets appear to track the electronics box and outboard sensor temperatures, rising and falling in the same cycle (Fig. 16).

As mentioned previously, the calibrated spin-plane gains for all spacecraft exhibited cyclical trends in Range 2 that merit individual visual comparison with instrument parameters extracted from telemetry. The spin-plane gains for C1 are the least affected by exceptional single-orbit fluctuations and have thus been chosen for comparison with the electronics box and outboard sensor temperatures as shown in Fig. 17 and Fig. 18.

Visual inspection of the plots indicates that there may be a correlation between the warming/cooling temperature cycles and cycling of the spin-plane gain fluctuation. In future, it might be desirable to perform a more thorough data correlation between calibration parameters and temperatures in order to try and discover a temperature coefficient which could be compared with ground data. This was deemed beyond the scope of the present work as an initial survey of parameter comparisons.

4 Conclusions and future work

The Cluster mission marks the first time that the magnetometer data from four spacecraft have been calibrated simultaneously in-flight. The FGM measurements, and the parameters determined by the FGM post-launch support team for calibrating the outboard magnetometer sensor, span over eleven years. The offsets on C1 show a steady drift in all ranges (for which there is sufficient data) at the resolution of spacecraft orbits over the course of the Cluster mission to February 2012. The offsets on C2, C3 and C4 remain fairly constant across all ranges. Cyclical trends in the calibration parameters that may be correlated with instrument house-keeping parameters have been identified. Examination of the tabulated means and standard deviations for the gains, elevation and azimuthal angles, has helped to identify cases in which the calibration

GID
4, 43–84, 2014

of certain archived orbits may need to be revisited. However, in general the stability of the outboard sensor calibration parameters over the course of the mission is excellent. Hence, confidence can be placed in the relative accuracy of the Cluster magnetic field data. In future papers, the features observed in the instrument house-keeping and calibration parameters will be explored further.

Acknowledgements. The Cluster FGM team would like to acknowledge ESA and the CAA for the ongoing operations and archiving support to fund this work. We acknowledge STFC for support until UK funding ceased in 2010. We thank IGeP Tu-BS for provision of the FGM data processing software. Finally, we express our regret for the loss of our valuable and respected colleague, Edita Georgescu.

References

Auster, H. U., Glassmeier, K. H., Magnes, W., Aydogar, O., Baumjohann, W., Constantinescu, D., Fischer, D., Fornacon, K. H., Georgescu, E., Harvey, P., Hillenmaier, O., Kroth, R., Ludlam, M., Narita, Y., Nakamura, R., Okrafka, K., Plaschke, F., Richter, I., Schwarzl, H., Stoll, B., Valavanoglou, A., and Wiedemann, M.: The THEMIS fluxgate magnetometer, Space Sci. Rev., 141, 235–264, 2008.

Balogh, A., Dunlop, M. W., Cowley, S. W. H., Southwood, D. J., Thomlinson, J. G., Glassmeier, K. H., Musmann, G., Lühr, H., Buchert, S., Acuña, M. H., Fairfield, D. H., Slavin, J. A., Riedler, W., Schwingenschuh, K., and Kivelson, M. G.: The Cluster Magnetic Field Investigation, Space Sci. Rev., 79, 65–91, 1997.

Escoubet, C. P., Russell, C. T., and Schmidt, R. (Eds.): The Cluster and Phoenix Missions, Kluwer Academic Publishers, Dordrecht, 1997.

Brown, P., Carr, C. M., Balogh, A., and Oddy, T. M.: FGM Instrument Users Manual, European Space Agency, 2000.

Gloag, J. M., Lucek, E. A., Alconcel, L. N., Balogh, A., Brown, P., Carr, C. M., Dunford, C. N., Oddy, T and Soucek, J.: FGM Data Products in the CAA, Cluster Active Archive: Studying the Earth's space plasma environment, Springer, New York, 109–128, 2010.

Hedgecock, P. C.: A correlation technique for magnetometer zero level determination, Space Sci. Inst., 1, 83–90, 1975.

GID

4, 43–84, 2014

Kepko, E. L., Khurana, K. K., Kivelson, M. G., Elphic, R. C., and Russell, C. T.: Accurate Determination of Magnetic Field Gradients from Four Point Vector Measurements – Part I: Use of Natural Constraints on Vector Data Obtained From a Single Spinning Spacecraft, IEEE T. Magn., 32, 377–385, 1996.

Laakso, H., Taylor, M. G. T., and Escoubet, C. P.: Cluster Active Archive: Studying the Earth's Space Plasma Environment, Springer, New York, 2010.

Walsh, A. P., Forsyth, C., Fazakerley, A. N., Chen, C. H. K., Lucek, E. A., Davies, J. A., Perry, C. H., Walker, S. N., and Balikhin, M. A.: 10 yr of the Cluster mission, Astron. Geophys., 51, 33–36, 2010.

Yin, F. and Luehr, H.: Recalibration of the CHAMP satellite magnetic field measurements, Meas. Sci. Technol., 22, 055101, doi:10.1088/0957-0233/22/5/055101, 2011.

GID

4, 43–84, 2014

Table 1. FGM instrument ranges.

Range Number	B
2	−64 to 63.97 nT
3	−256 to 255.87 nT
4	−1024 to 1023.5 nT
5	−4096 to 4094 nT
6	−16 384 to 16 376 nT
7	−65 536 to 65 504 nT

GID
4, 43–84, 2014

Table 2. Mean and standard deviation of the offsets (O_i) for the mission segment February 2001 to February 2012 for each coordinate in every range on all spacecraft. Standard deviations for ranges that are at least twice as large as those for all the other spacecraft in that range are highlighted.

Offset [nT]													
Mean							Standard Deviation						
Coordinate X (Spin Axis)							Coordinate X (Spin Axis)						
	Range 2	Range 3	Range 4	Range 5	Range 6	Range 7		Range 2	Range 3	Range 4	Range 5	Range 6	Range 7
Cluster 1	−3.6472	−3.6369	−47.7928	−54.3448	−673.5400	−674.4603	Cluster 1	0.6766	0.6640	7.1821	2.4061	9.0951	3.0666
Cluster 2	−0.0500	−0.0152	2.6330	3.7948	35.2962	53.7593	Cluster 2	0.1584	0.2381	0.2476	0.1306	1.5797	2.6602
Cluster 3	−2.2598	−2.2524	3.9283	4.9363	102.3391	117.9678	Cluster 3	0.1901	0.2177	0.2859	0.2486	2.0647	7.1798
Cluster 4	−12.4734	−12.6754	−4.8021	−4.3011	139.0179	148.3692	Cluster 4	0.1601	0.2154	0.2730	0.2344	1.3255	0.9424
Coordinate Y (Spin Plane)							Coordinate Y (Spin Plane)						
	Range 2	Range 3	Range 4	Range 5	Range 6	Range 7		Range 2	Range 3	Range 4	Range 5	Range 6	Range 7
Cluster 1	6.3769	6.5161	23.5516	27.0978	290.7744	306.5775	Cluster 1	0.8277	0.8612	2.9593	1.1031	4.6518	0.8060
Cluster 2	−2.4250	−2.4275	−2.3179	−1.9333	−9.1467	−1.4474	Cluster 2	0.1352	0.1354	0.1720	0.1972	1.8764	0.5007
Cluster 3	−5.0619	−5.0893	1.4972	2.5117	107.5918	123.1750	Cluster 3	0.1608	0.1806	0.2780	0.1713	1.4813	1.1888
Cluster 4	−3.0896	−3.0820	3.4234	4.4197	118.6630	136.0400	Cluster 4	0.1226	0.1301	0.1916	0.2587	1.8519	1.4878
Coordinate Z (Spin Plane)							Coordinate Z (Spin Plane)						
	Range 2	Range 3	Range 4	Range 5	Range 6	Range 7		Range 2	Range 3	Range 4	Range 5	Range 6	Range 7
Cluster 1	0.3404	0.3902	−3.7819	−4.2444	−45.3345	−30.1555	Cluster 1	0.4079	0.4161	1.4741	0.7021	2.2685	0.4895
Cluster 2	−1.3266	−1.2949	−0.7288	−0.2202	−0.3983	9.7505	Cluster 2	0.1898	0.1946	0.2567	0.2278	1.5767	0.8130
Cluster 3	−2.5431	−2.5588	2.4850	3.0053	90.8152	101.4771	Cluster 3	0.1376	0.1408	0.2026	0.1634	2.4599	1.8917
Cluster 4	4.4047	4.5053	12.7467	13.3045	156.8103	166.8212	Cluster 4	0.1780	0.1867	0.1862	0.1681	1.8072	1.2587

GID
4, 43–84, 2014

Table 3. Mean and standard deviation of gains (G_1 and ΔG_{32}) for the mission segment February 2001 to February 2012 for each coordinate in every range on all spacecraft. Standard deviations for ranges that are at least twice as large as those for all the other spacecraft in that range are highlighted.

Gain													
Mean							Standard Deviation						
Coordinate X (Spin Axis)							Coordinate X (Spin Axis)						
	Range 2	Range 3	Range 4	Range 5	Range 6	Range 7		Range 2	Range 3	Range 4	Range 5	Range 6	Range 7
Cluster 1	0.9501	0.9684	0.9790	0.9962	0.9768	0.9978	Cluster 1	0.0037	0.0024	0.0063	0.0001	0.0046	0.0031
Cluster 2	0.9586	0.9759	0.9866	1.0034	0.9853	1.0012	Cluster 2	0.0037	0.0007	0.0010	0.0001	0.0027	0.0007
Cluster 3	0.9600	0.9756	0.9954	1.0110	0.9953	1.0101	Cluster 3	0.0033	0.0010	0.0010	0.0001	0.0068	0.0025
Cluster 4	0.9595	0.9783	0.9954	1.0130	0.9925	1.0108	Cluster 4	0.0032	0.0008	0.0002	0.0001	0.0010	0.0019
Coordinate Y/Coordinate Z (Spin Plane)							Coordinate Y/Coordinate Z (Spin Plane)						
	Range 2	Range 3	Range 4	Range 5	Range 6	Range 7		Range 2	Range 3	Range 4	Range 5	Range 6	Range 7
Cluster 1	0.9838	0.9846	0.9892	0.9901	0.9915	0.9930	Cluster 1	0.0008	0.0006	0.0001	0.0000	0.0000	0.0015
Cluster 2	1.0060	1.0069	0.9959	0.9969	0.9950	0.9960	Cluster 2	0.0007	0.0003	0.0002	0.0000	0.0000	0.0000
Cluster 3	1.0190	1.0169	1.0133	1.0112	1.0106	1.0085	Cluster 3	0.0005	0.0003	0.0001	0.0001	0.0001	0.0001
Cluster 4	0.9741	0.9752	0.9730	0.9741	0.9758	0.9769	Cluster 4	0.0004	0.0003	0.0001	0.0001	0.0001	0.0001

GID
4, 43–84, 2014

Table 4. Mean and standard deviation of elevation angles (θ_i) for the mission segment February 2001 to February 2012 in every range on all spacecraft. Standard deviations for ranges that are at least twice as large as those for all the other spacecraft in that range are highlighted.

Theta [deg]													
Mean							Standard Deviation						
Coordinate *X* (Spin Axis)							Coordinate *X* (Spin Axis)						
	Range 2	Range 3	Range 4	Range 5	Range 6	Range 7		Range 2	Range 3	Range 4	Range 5	Range 6	Range 7
Cluster 1	0.7885	0.7712	0.7690	0.7708	0.7585	0.7525	Cluster 1	0.0463	0.0126	0.0264	0.0785	0.0054	0.0145
Cluster 2	0.3810	0.3669	0.3674	0.3709	0.3645	0.3584	Cluster 2	0.0249	0.0060	0.0049	0.0030	0.0038	0.0036
Cluster 3	0.8345	0.8232	0.8242	0.8222	0.8269	0.8268	Cluster 3	0.0228	0.0073	0.0038	0.0026	0.0020	0.0017
Cluster 4	0.3323	0.3216	0.3352	0.3301	0.3564	0.3445	Cluster 4	0.0200	0.0102	0.0083	0.0048	0.0084	0.0030
Coordinate *Y* (Spin Plane)							Coordinate *Y* (Spin Plane)						
	Range 2	Range 3	Range 4	Range 5	Range 6	Range 7		Range 2	Range 3	Range 4	Range 5	Range 6	Range 7
Cluster 1	90.1757	90.1731	90.1919	90.1667	90.1940	90.2104	Cluster 1	0.1831	0.2995	0.0522	0.0160	0.0144	0.0045
Cluster 2	89.4633	89.4644	89.4575	89.4572	89.4710	89.4660	Cluster 2	0.1162	0.1366	0.0180	0.0080	0.0232	0.0060
Cluster 3	89.5477	89.5163	89.5268	89.5276	89.5205	89.5170	Cluster 3	0.1426	0.1649	0.0147	0.0060	0.0178	0.0123
Cluster 4	89.5849	89.5747	89.5695	89.5703	89.5654	89.5661	Cluster 4	0.0920	0.1473	0.0139	0.0088	0.0173	0.0056
Coordinate *Z* (Spin Plane)							Coordinate *Z* (Spin Plane)						
	Range 2	Range 3	Range 4	Range 5	Range 6	Range 7		Range 2	Range 3	Range 4	Range 5	Range 6	Range 7
Cluster 1	90.3697	90.3718	90.3484	90.3567	90.3604	90.3441	Cluster 1	0.2282	0.3353	0.0355	0.0095	0.0087	0.0105
Cluster 2	89.9023	89.8835	89.9163	89.9048	89.9416	89.9405	Cluster 2	0.1784	0.2641	0.0290	0.0122	0.0226	0.0072
Cluster 3	89.7856	89.7891	89.7895	89.7908	89.7961	89.7944	Cluster 3	0.0852	0.0938	0.0147	0.0046	0.0204	0.0144
Cluster 4	90.1174	90.1102	90.1472	90.1448	90.1573	90.1642	Cluster 4	0.1012	0.1989	0.0190	0.0093	0.0157	0.0032

GID
4, 43–84, 2014

Table 5. Mean and standard deviation of azimuthal angles (ϕ_1 and $\Delta\phi_{32}$) for the segment February 2001 to February 2012 in every range on all spacecraft. Standard deviations for ranges that are at least twice as large as those for all the other spacecraft in that range are highlighted.

Phi [deg]													
Mean								Standard Deviation					
Coordinate *X* (Spin Axis)								Coordinate *X* (Spin Axis)					
	Range 2	Range 3	Range 4	Range 5	Range 6	Range 7		Range 2	Range 3	Range 4	Range 5	Range 6	Range 7
Cluster 1	−119.1660	−119.7569	−119.8577	−119.2300	−120.2909	−120.1777	Cluster 1	3.0226	1.1705	1.9420	4.6769	0.4280	0.8844
Cluster 2	−64.0525	−64.6089	−64.7972	−64.0862	−63.5864	−62.9272	Cluster 2	3.1645	1.5030	1.0622	0.5746	0.6301	0.5993
Cluster 3	167.2952	167.3242	167.4878	167.3291	167.6715	167.6313	Cluster 3	8.3095	0.4849	0.4442	0.2916	0.1733	0.0578
Cluster 4	−89.3505	−89.6458	−89.6609	−88.8032	−88.5315	−88.1017	Cluster 4	3.0891	2.2719	1.3100	1.0304	0.5087	0.3351
Coordinate *Y* (Spin Plane)								Coordinate *Y* (Spin Plane)					
	Range 2	Range 3	Range 4	Range 5	Range 6	Range 7		Range 2	Range 3	Range 4	Range 5	Range 6	Range 7
Cluster 1	0.0001	0.0013	0.0274	0.0393	0.1818	0.0635	Cluster 1	0.0013	0.0459	0.0997	0.1016	0.1660	0.1134
Cluster 2	0.0010	0.0013	0.0328	−0.0410	−0.0696	−0.0511	Cluster 2	0.0081	0.0528	0.1211	0.1029	0.0499	0.0581
Cluster 3	0.0006	−0.0005	0.0430	−0.0435	−0.1531	−0.0416	Cluster 3	0.0070	0.0672	0.1727	0.1325	0.4112	0.0606
Cluster 4	0.0011	0.0101	0.0432	−0.0319	−0.0684	−0.0241	Cluster 4	0.0140	0.0554	0.1207	0.1095	0.0632	0.0413
Coordinate *Z* (Spin Plane)								Coordinate *Z* (Spin Plane)					
	Range 2	Range 3	Range 4	Range 5	Range 6	Range 7		Range 2	Range 3	Range 4	Range 5	Range 6	Range 7
Cluster 1	89.7587	89.7515	89.5710	89.6108	89.7017	89.5812	Cluster 1	0.0952	0.0829	0.1055	0.1056	0.1661	0.1132
Cluster 2	89.3720	89.3711	89.3945	89.3249	89.2996	89.3124	Cluster 2	0.0312	0.0579	0.1187	0.1024	0.0519	0.0592
Cluster 3	89.2567	89.2544	89.3611	89.2748	89.1769	89.2846	Cluster 3	0.0297	0.0685	0.1719	0.1327	0.4108	0.0614
Cluster 4	88.8329	88.8426	88.8633	88.7933	88.7583	88.7993	Cluster 4	0.0265	0.0585	0.1168	0.1087	0.0648	0.0432

GID
4, 43–84, 2014

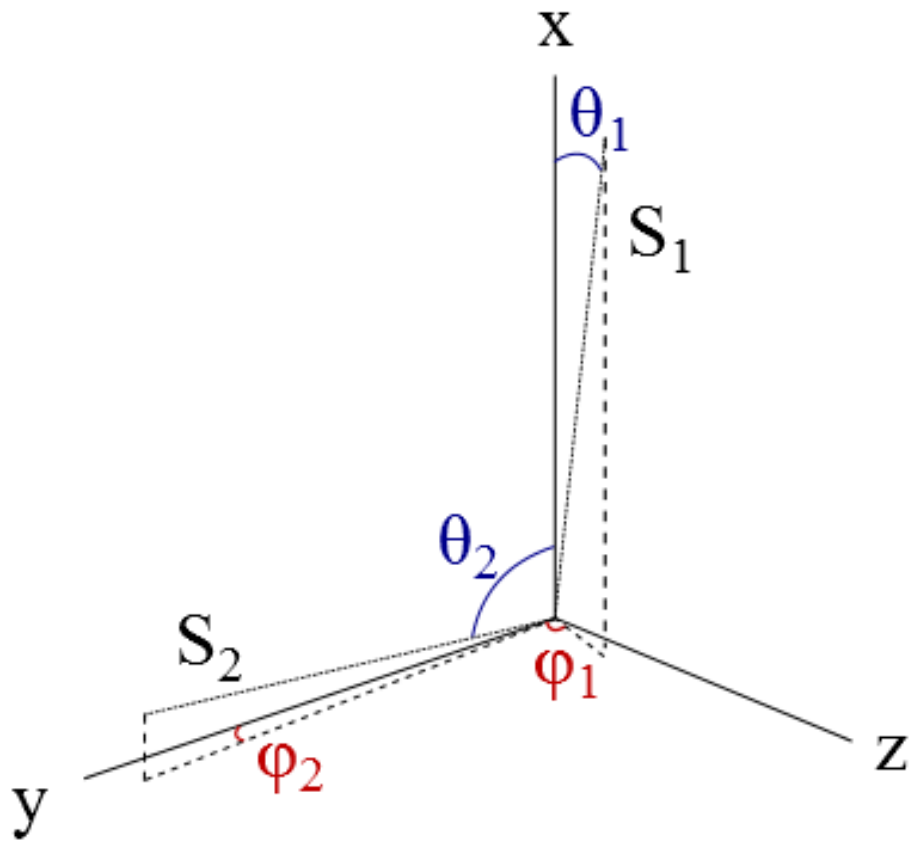

Fig. 1. The relation between the orthogonal (x, y, z) and sensor (S_1, S_2, S_3) coordinate systems. The elevation and azimuthal angles θ and ϕ for each sensor coordinate are defined in the same way. S_3 has been omitted for clarity.

GID
4, 43–84, 2014

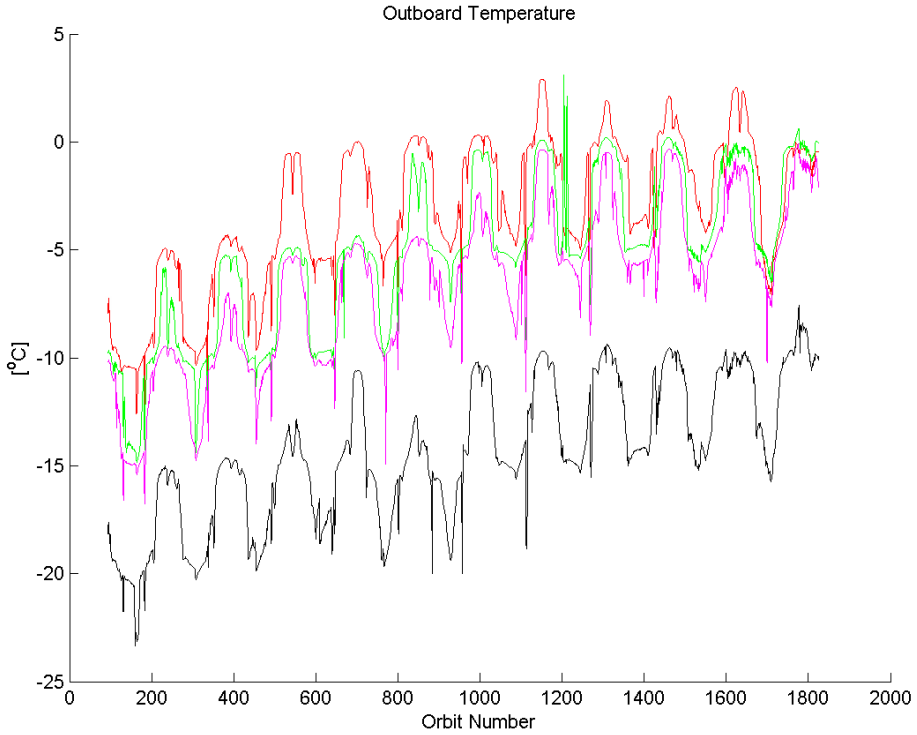

Fig. 2. Outboard sensor temperatures in degrees Celsius for each spacecraft for Orbits 93 to 1889 (February 2001 through August 2012). C1 = black, C2 = red, C3 = green, C4 = magenta.

GID
4, 43–84, 2014

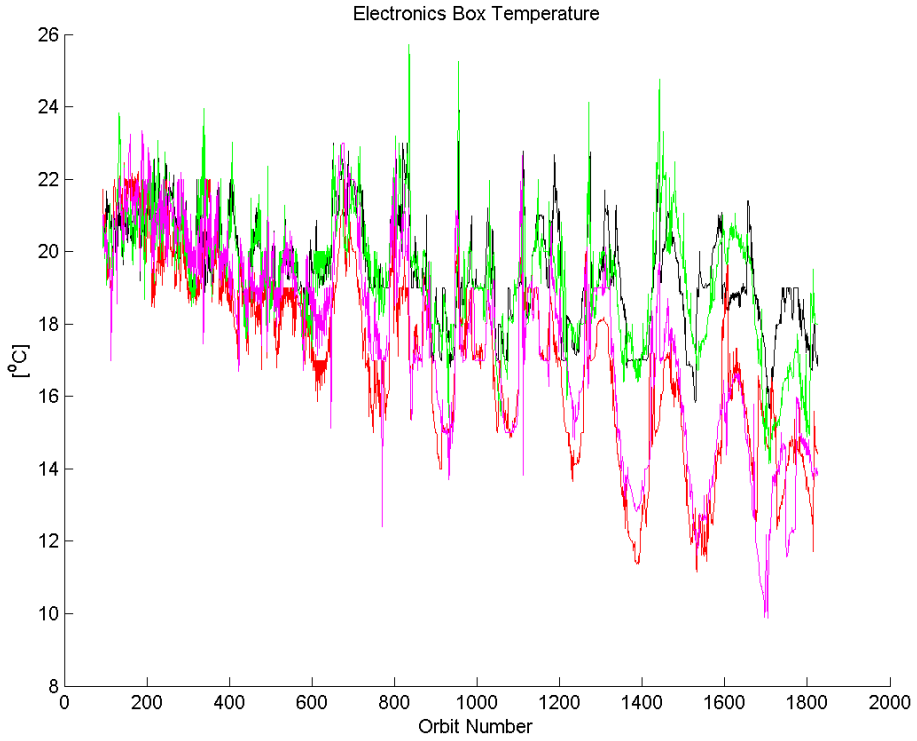

Fig. 3. Electronics box temperatures in degrees Celsius for each spacecraft for Orbits 93 to 1889 (February 2001 through August 2012). C1 = black, C2 = red, C3 = green, C4 = magenta.

GID
4, 43–84, 2014

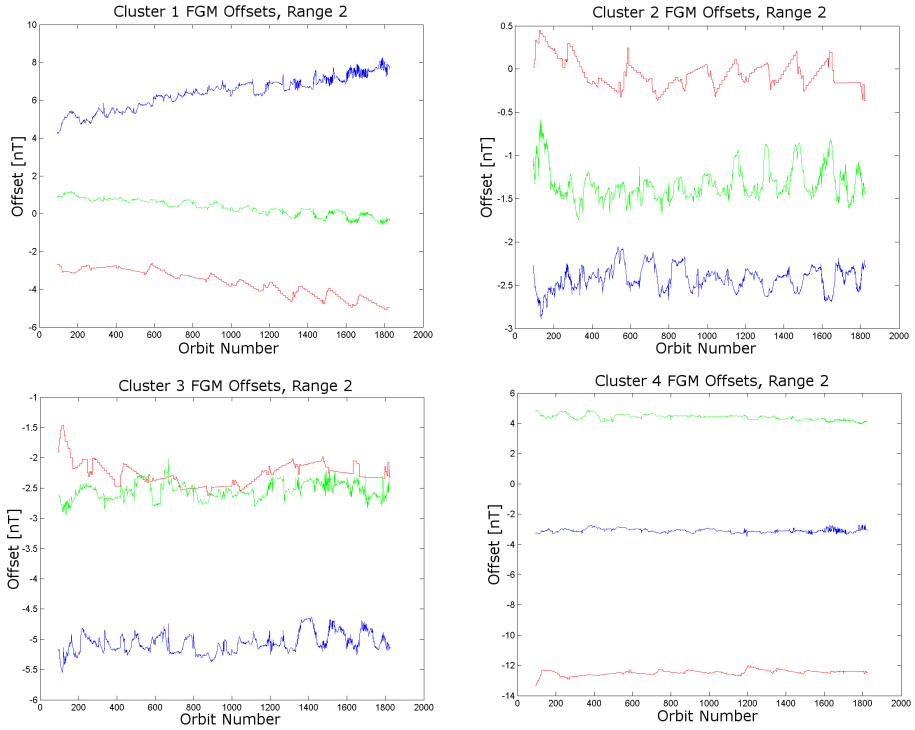

Fig. 4. Range 2 spin-axis (O_1, red) and spin-plane (O_2 and O_3, blue and green) offsets in nT for Orbits 93 through 1825 (February 2001 through February 2012).

GID
4, 43–84, 2014

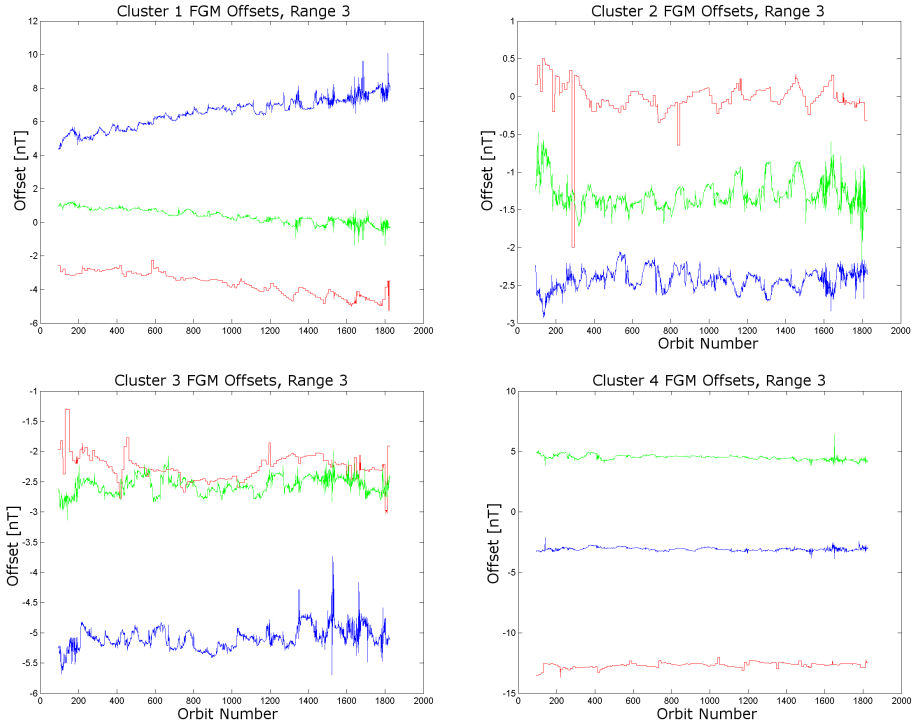

Fig. 5. Range 3 spin-axis (O_1, red) and spin-plane (O_2 and O_3, blue and green) offsets in nT for Orbits 93 through 1825 (February 2001 through February 2012).

GID
4, 43–84, 2014

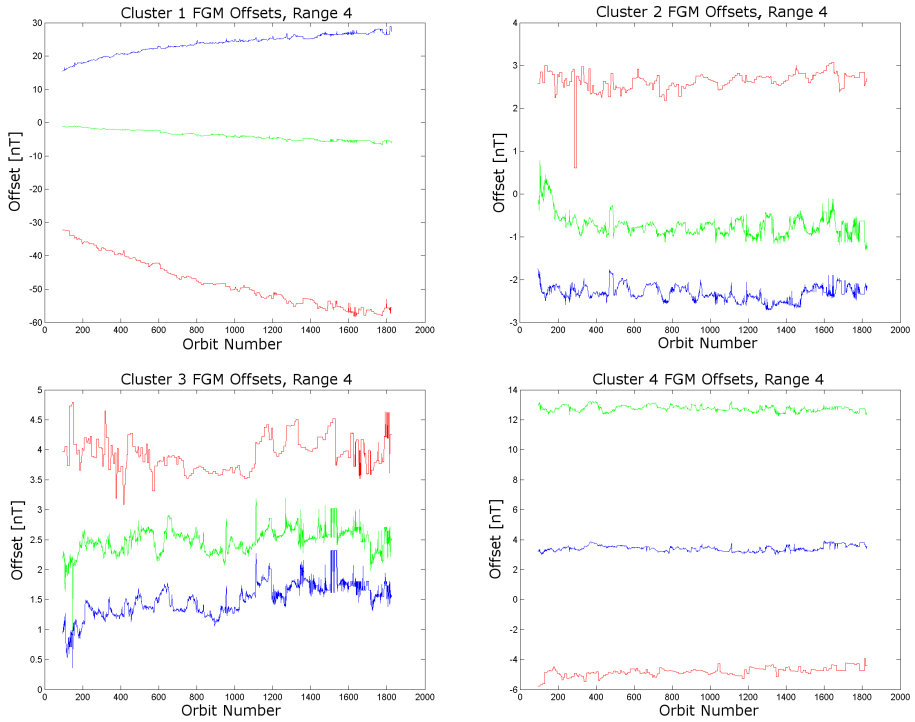

Fig. 6. Range 4 spin-axis (O_1, red) and spin-plane (O_2 and O_3, blue and green) offsets in nT for Orbits 93 through 1825 (February 2001 through February 2012).

GID
4, 43–84, 2014

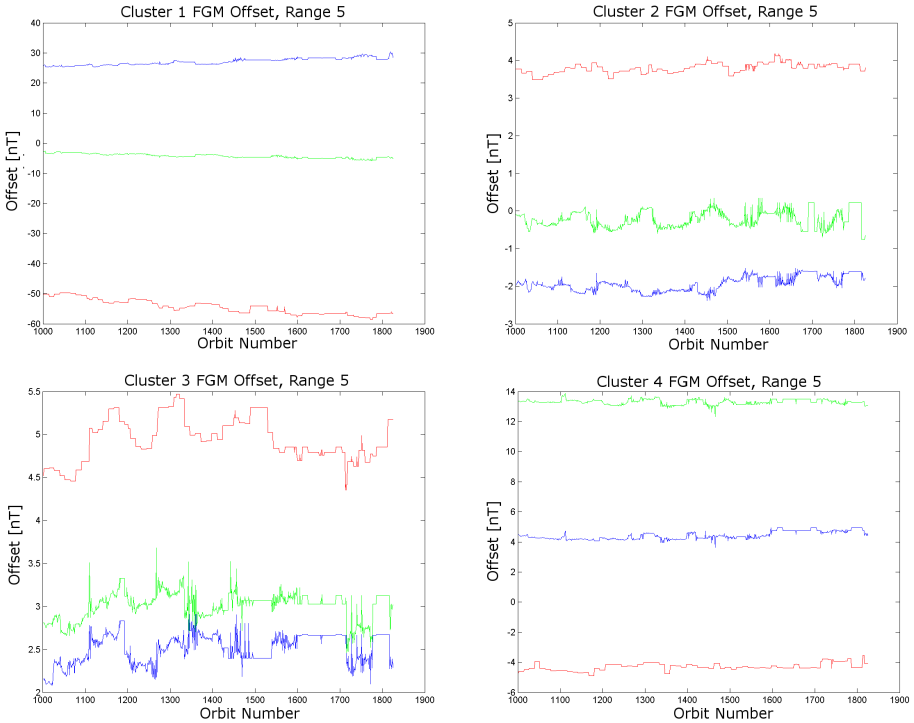

Fig. 7. Range 5 spin-axis (O_1, red) and spin-plane (O_2 and O_3, blue and green) offsets in nT for Orbits 1000 through 1812 (December 2006 through February 2012).

GID
4, 43–84, 2014

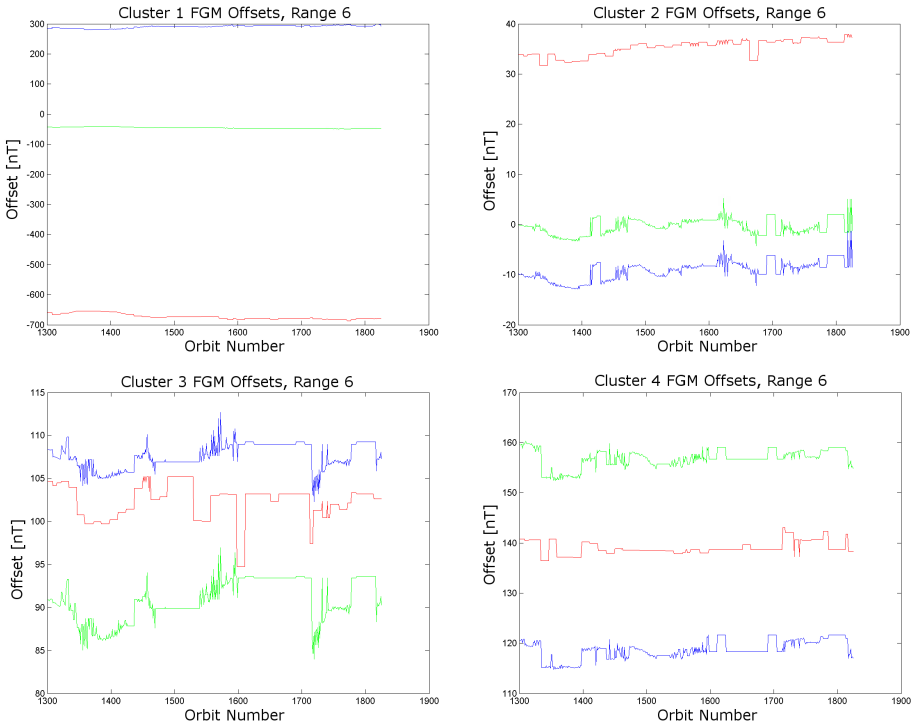

Fig. 8. Range 6 spin-axis (O_1, red) and spin-plane (O_2 and O_3, blue and green) offsets in nT for Orbits 1300 through 1825 (December 2008 through February 2012).

GID
4, 43–84, 2014

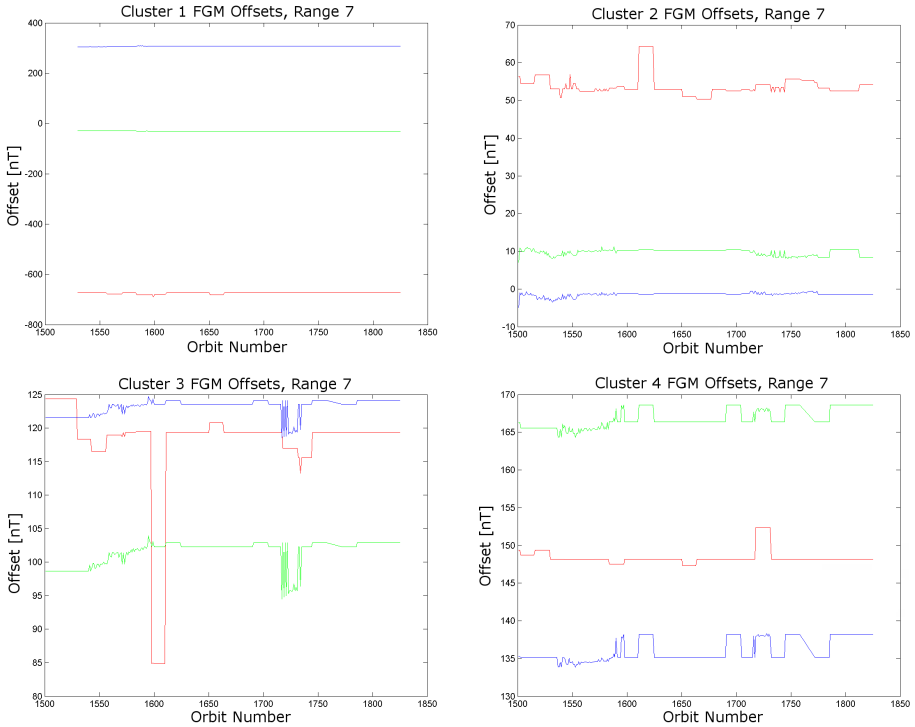

Fig. 9. Range 7 spin-axis (O_1, red) and spin-plane (O_2 and O_3, blue and green) offsets in nT for Orbits 1445 through 1825 (December 2009 through February 2012).

GID
4, 43–84, 2014

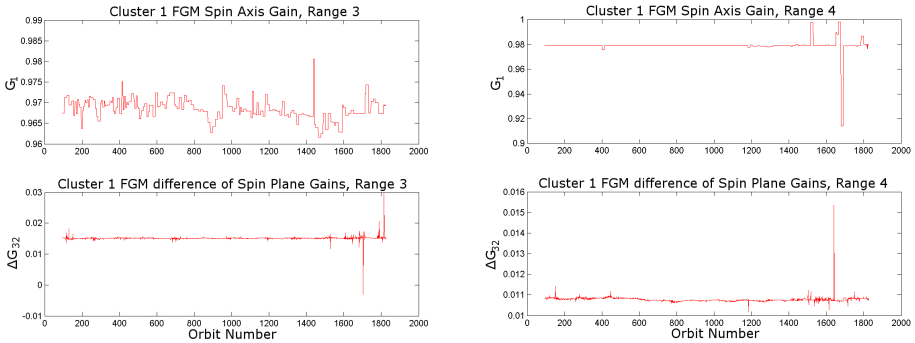

Fig. 10. Gain plots (G_1 and ΔG_{32}) from February 2001 to February 2012 for exceptional cases in C1.

GID
4, 43–84, 2014

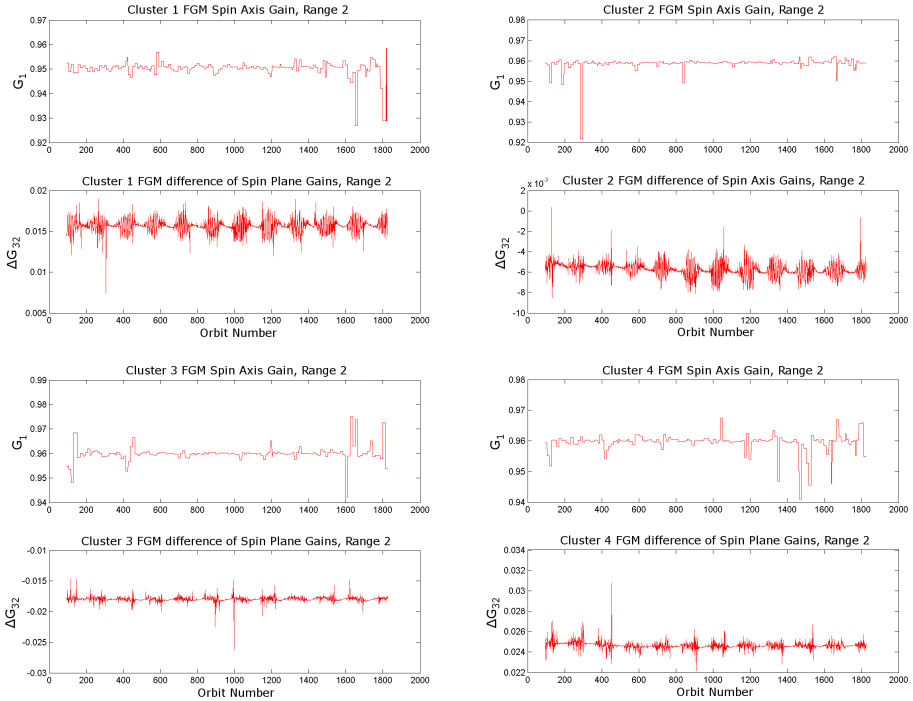

Fig. 11. Gain plots (G_1 and ΔG_{32}) from Feburary 2001 to February 2012 showing periodic behaviour of spin-plane gain difference for Range 2 in all spacecraft.

GID
4, 43–84, 2014

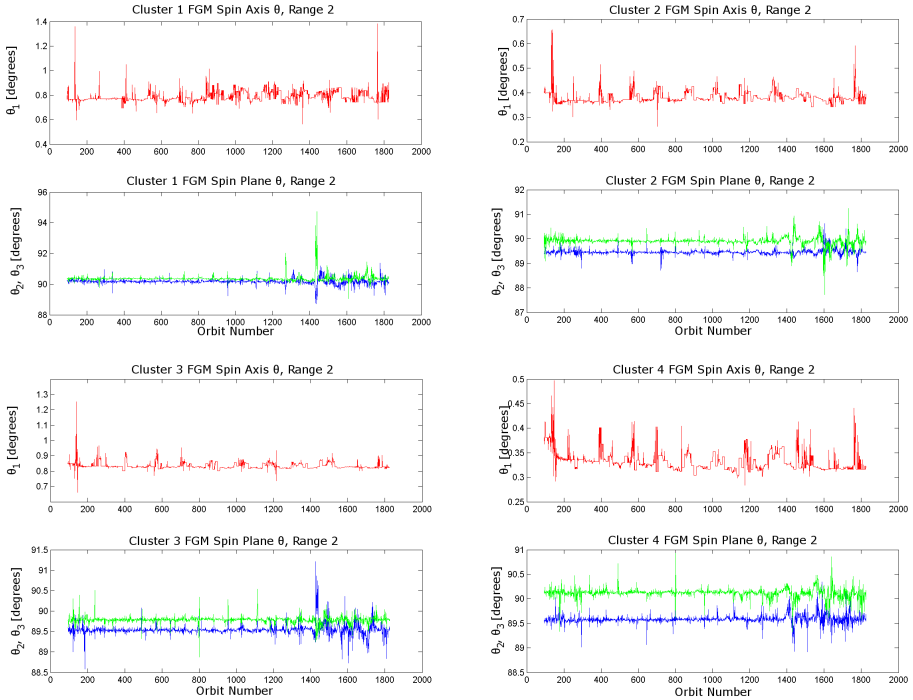

Fig. 12. Elevation angle, θ_i, plots for February 2001 to February 2012 for Range 2 for all spacecraft.

GID
4, 43–84, 2014

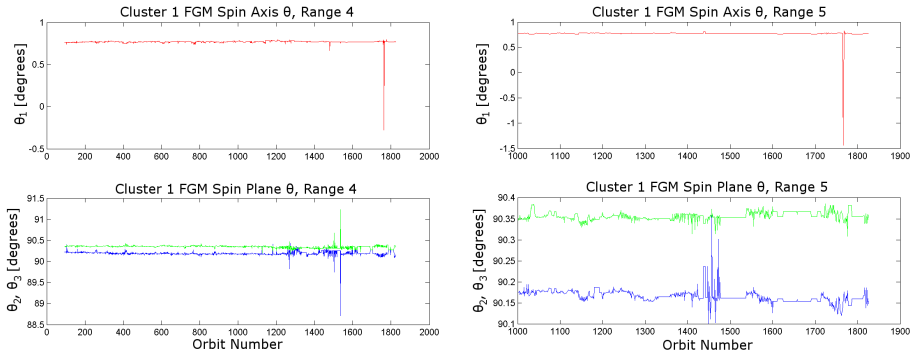

Fig. 13. Elevation angle, θ_i, plots for C1, Ranges 4 and 5, for February 2001 to February 2012.

GID
4, 43–84, 2014

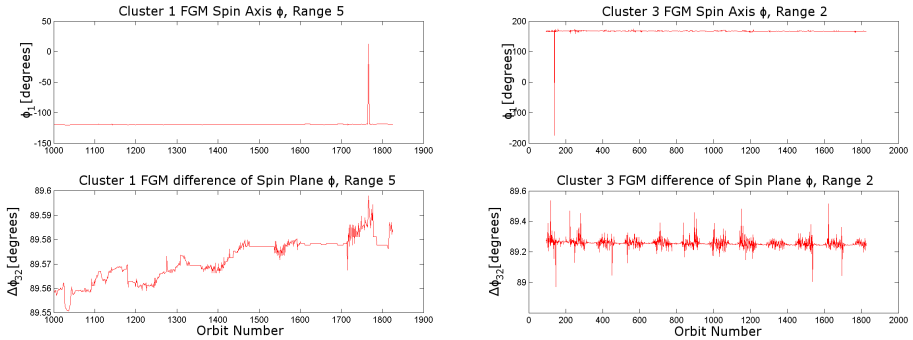

Fig. 14. Azimuthal angles, ϕ_1 and $\Delta\phi_{32}$, for C1, Range 5 and C3, Range 2.

GID
4, 43–84, 2014

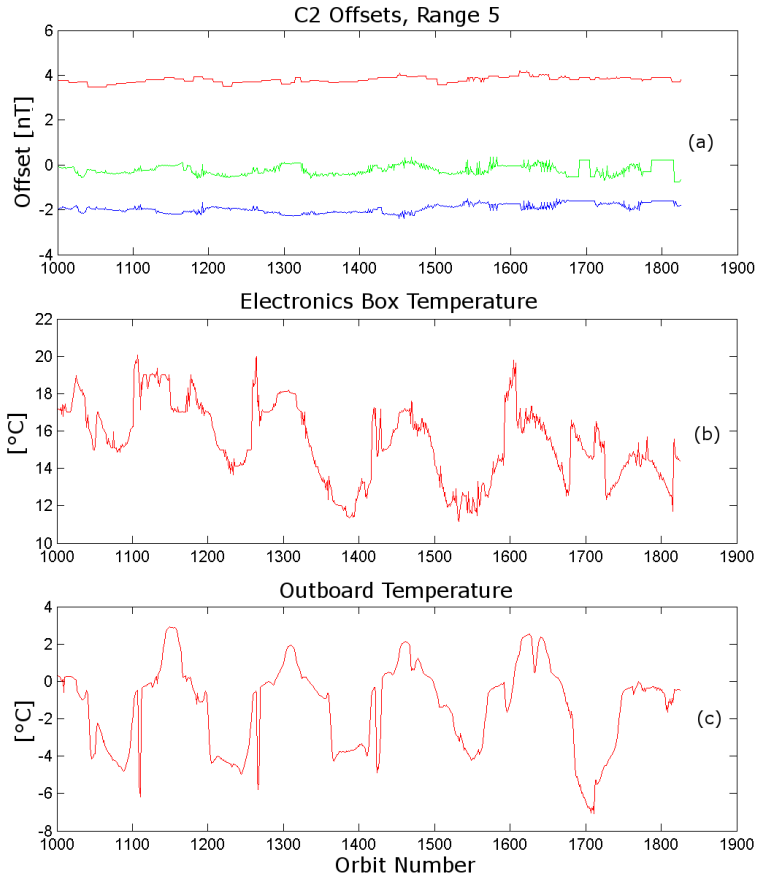

Fig. 15. Panel **(a)** C2 Range 5 offsets (O_1 in red, O_2 in blue and O_3 in green), panel **(b)** C2 electronics box temperature and panel **(c)** C2 outboard sensor temperature. Offsets shown in nT and temperatures in °C for Orbits 1000 through 1812 (December 2006 through February 2012).

GID
4, 43–84, 2014

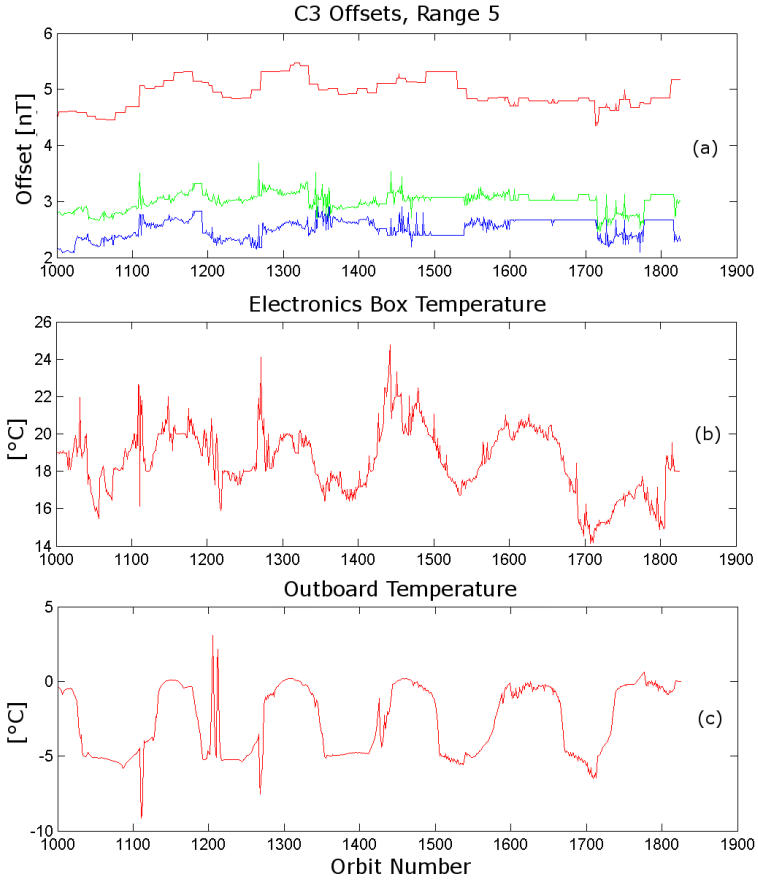

Fig. 16. Panel **(a)** C3 Range 5 offsets (O_1 in red, O_2 in blue and O_3 in green), panel **(b)** C3 electronics box temperature and panel **(c)** C3 outboard sensor temperature. Offsets shown in nT and temperatures in °C for Orbits 1000 through 1825 (December 2006 through February 2012).

GID
4, 43–84, 2014

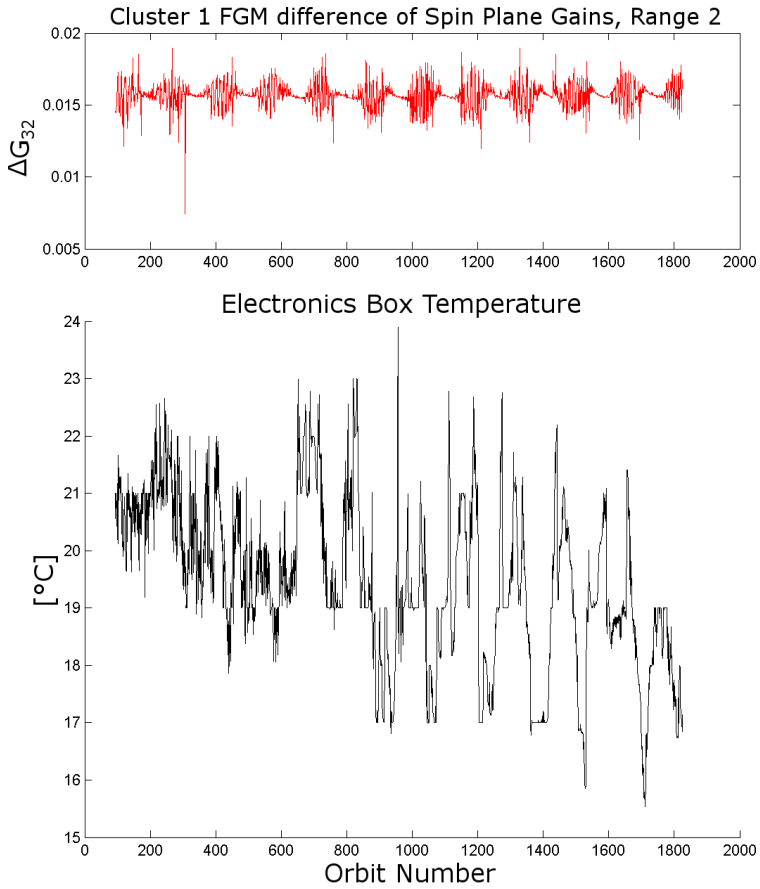

Fig. 17. Spin-plane gain difference (ΔG_{32}) for C1, Range 2 and electronics box temperatures in °C for Orbits 93 through 1825 (February 2001 through February 2012).

GID
4, 43–84, 2014

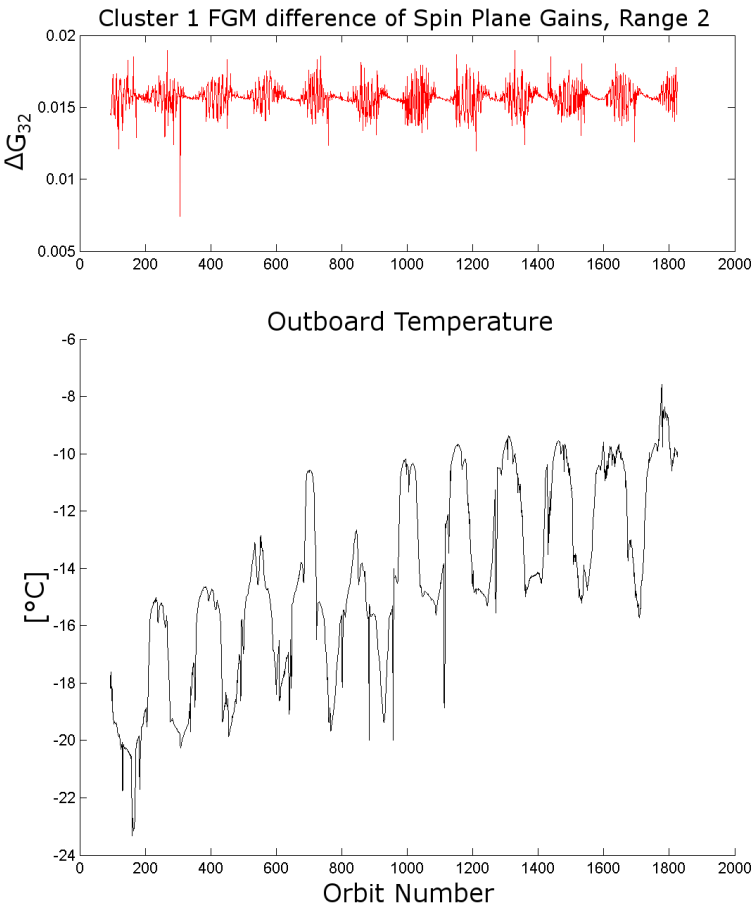

Fig. 18. Spin-plane gain difference (ΔG_{32}) for C1, Range 2 and sensor temperatures in °C for Orbits 93 through 1825 (February 2001 through February 2012).

GID
4, 43–84, 2014